Electronic Supplementary Material (ESI) for Journal of Materials Chemistry A.

# ***Supplementary information***

**Title:** $NO_X$ reduction consequences of lanthanide-substituted vanadates functionalized with S or P poisons under oxidative environments†

**Authors:** Hyo Jin An,‡ Dong Ho Kim,‡ Heon Phil Ha,* and Jongsik Kim*

‡ These authors are contributed equally to this work.

## Table of Contents

**Table S1**. Logarithmic acid dissociation (p$K_A$) and base association constants (p$K_B$) of $HSO_A^-/SO_A^{2-}$ (A= 3 or 4) and $H_{3-B}PO_4^{B-}$ species (B= 1, 2, or 3).

| chemical equilibrium [a] | p$K_A$ [b] | p$K_B$ [b] |
|---|---|---|
| $H_2PO_4^- + H^+ \rightleftarrows H_3PO_4$ | 2.1 | 11.9 |
| $HPO_4^{2-} + H^+ \rightleftarrows H_2PO_4^-$ | 7.2 | 6.8 |
| $PO_4^{3-} + H^+ \rightleftarrows HPO_4^{2-}$ | 12.3 | 1.7 |
| $HSO_4^- + H^+ \rightleftarrows H_2SO_4$ | -3 | 17.0 |
| $SO_4^{2-} + H^+ \rightleftarrows HSO_4^-$ | 1.9 | 12.1 |
| $HSO_3^- + H^+ \rightleftarrows H_2SO_3$ | 1.8 | 12.2 |
| $SO_3^{2-} + H^+ \rightleftarrows HSO_3^-$ | 7.2 | 6.8 |

[a] at 25 °C and 1 bar. [b] p$K_W$= p$K_A$ + p$K_B$, where $K_W$ is self-ionization constant of $H_2O$.

**Table S2**. Properties of the catalysts.

| catalyst | $S_{BET}$ [a] ($m^2$ $g_{CAT}^{-1}$) | $V_{BJH}$ [a] ($cm^3$ $g_{CAT}^{-1}$) | RM/V [b] | | S (or P)/(RM+V) [b] | |
|---|---|---|---|---|---|---|
| | | | bulk [c, d] | surface [e] | bulk [d] | surface [e] |
| Ce-S | 64.97 | 0.25 | 1.01 (± 0.03) | 0.97 (± 0.01) | 0.42 (± 0.05) | 0.52 (± 0.01) |
| Nd-S | 68.51 | 0.21 | 1.01 (± 0.03) | 1.07 (± 0.01) | 0.44 (± 0.06) | 0.52 (± 0.01) |
| Sm-S | 64.51 | 0.29 | 1.04 (± 0.03) | 1.00 (± 0.01) | 0.39 (± 0.05) | 0.49 (± 0.01) |
| Gd-S | 68.91 | 0.26 | 0.98 (± 0.02) | 1.07 (± 0.01) | 0.41 (± 0.06) | 0.50 (± 0.01) |
| Tb-S | 67.59 | 0.27 | 1.02 (± 0.04) | 0.99 (± 0.01) | 0.40 (± 0.06) | 0.51 (± 0.01) |
| Er-S | 63.03 | 0.30 | 1.02 (± 0.03) | 1.01 (± 0.01) | 0.38 (± 0.05) | 0.50 (± 0.01) |
| Ce-P | 68.84 | 0.25 | 1.02 (± 0.02) | 1.01 (± 0.02) | 0.51 (± 0.07) | 0.59 (± 0.01) |
| Nd-P | 72.11 | 0.19 | 1.02 (± 0.03) | 0.98 (± 0.07) | 0.51 (± 0.07) | 0.60 (± 0.03) |
| Sm-P | 73.65 | 0.29 | 0.99 (± 0.03) | 0.94 (± 0.02) | 0.50 (± 0.06) | 0.58 (± 0.04) |
| Gd-P | 70.74 | 0.26 | 0.96 (± 0.03) | 1.00 (± 0.02) | 0.53 (± 0.07) | 0.60 (± 0.05) |
| Tb-P | 66.15 | 0.25 | 0.99 (± 0.03) | 0.99 (± 0.02) | 0.52 (± 0.06) | 0.60 (± 0.02) |
| Er-P | 68.15 | 0.30 | 1.00 (± 0.03) | 0.99 (± 0.02) | 0.59 (± 0.08) | 0.60 (± 0.08) |

[a] via $N_2$ physisorption. [b] molar ratio. [c] bulk V contents of ~ 2wt. %. [d] via XRF. [e] via XP spectroscopy.

**Table S3**. Peak locations of the sub-bands assigned as surface $V^{3+}$, $V^{4+}$, or $V^{5+}$ species in the XP spectra of the catalysts.

| catalyst | Tb-S | Ce-S | Nd-S | Sm-S | Gd-S | Er-S |
|---|---|---|---|---|---|---|
| $V^{3+}$[a, c] (eV) | 515.20 | 515.25 | 515.31 | 515.36 | 515.42 | 515.50 |
| $V^{4+}$[a, c] (eV) | 516.08 | 516.13 | 516.18 | 516.24 | 516.30 | 516.40 |
| $V^{5+}$[a, c] (eV) | 516.86 | 516.92 | 516.98 | 517.06 | 517.12 | 517.20 |
| catalyst | Tb-P | Ce-P | Nd-P | Sm-P | Gd-P | Er-P |
| $V^{3+}$[b, c] (eV) | 515.15 | 515.21 | 515.27 | 515.33 | 515.40 | 515.45 |
| $V^{4+}$[b, c] (eV) | 516.00 | 516.05 | 516.11 | 516.17 | 516.26 | 516.35 |
| $V^{5+}$[b, c] (eV) | 516.80 | 516.84 | 516.93 | 517.00 | 517.08 | 517.15 |

[a] See Fig. S3A†. [b] See Fig. S3B†. [c] peak resolution of 0.05 eV.

**Table S4**. Slopes of the fittings used to calculate $NH_3$ binding energies ($E_{NH3}$) for the catalysts.

$NH_3$-TPD profiles post the saturation of the surfaces with $NH_3$ at 250 °C

| band | slope of the fitting [a] | | | | | |
|---|---|---|---|---|---|---|
| | Tb-S [c] | Ce-S [c] | Nd-S [c] | Sm-S [d] | Gd-S [d] | Er-S [d] |
| marked with 🔴 [b] | -3841.3 | -5007.8 | -4306.3 | -3812.4 | -4558.7 | -4037.6 |
| marked with 🟢 [b] | -3919.7 | -5186.1 | -4270.2 | -3930.6 | -4575.4 | -4156.1 |
| marked with 🔵 [b] | -3931.3 | -5139.1 | -4362.7 | -3936.5 | -4459.7 | -4061.1 |

| band | slope of the fitting [a] | | | | | |
|---|---|---|---|---|---|---|
| | Tb-P [e] | Ce-P [e] | Nd-P [e] | Sm-P [f] | Gd-P [f] | Er-P [f] |
| marked with 🔴 [b] | -3777.2 | -5009.6 | -4177.4 | -3892.0 | -4438.3 | -4006.5 |
| marked with 🟢 [b] | -3726.4 | -5080.7 | -4257.4 | -3820.6 | -4416.3 | -4040.3 |
| marked with 🔵 [b] | -3735.9 | -5031.0 | -4264.4 | -3824.5 | -4448.9 | -4011.3 |

$NH_3$-TPD profiles post the saturation of the surfaces with $NH_3$ at 350 °C

| band | slope of the fitting [a] | | | | | |
|---|---|---|---|---|---|---|
| | Tb-S [g] | Ce-S [g] | Nd-S [g] | Sm-S [h] | Gd-S [h] | Er-S [h] |
| marked with 🔴 [b] | -2828.6 | -4241.4 | -3445.4 | -2806.9 | -3681.9 | -3288.4 |
| marked with 🟢 [b] | -2786.2 | -4193.6 | -3370.9 | -2930.3 | -3469.1 | -3275.0 |

| band | slope of the fitting [a] | | | | | |
|---|---|---|---|---|---|---|
| | Tb-P [i] | Ce-P [i] | Nd-P [i] | Sm-P [j] | Gd-P [j] | Er-P [j] |
| marked with 🔴 [b] | -2560.4 | -3758.5 | -2903.2 | -2784.3 | -3344.9 | -2659.7 |
| marked with 🟢 [b] | -2476.4 | -3746.0 | -2920.8 | -2743.2 | -3378.9 | -2619.3 |

[a] use of peak temperatures ($T_M$) obtained through $NH_3$-TPD experiments at the ramping rates (β) of 10 °C $min^{-1}$, 20 °C $min^{-1}$, and 30 °C $min^{-1}$; regression factors ($R^2$) of ≥ 0.99. [b] peak temperature ($T_M$). [c] See Fig. S7 and S15A†. [d] See Fig. S8 and S15A†. [e] See Fig. S9 and S15B†. [f] See Fig. S10 and S15B†. [g] See Fig. S11 and S15C†. [h] See Fig. S12 and S15C†. [i] See Fig. S13 and S15D†. [j] See Fig. S14 and S15D†.

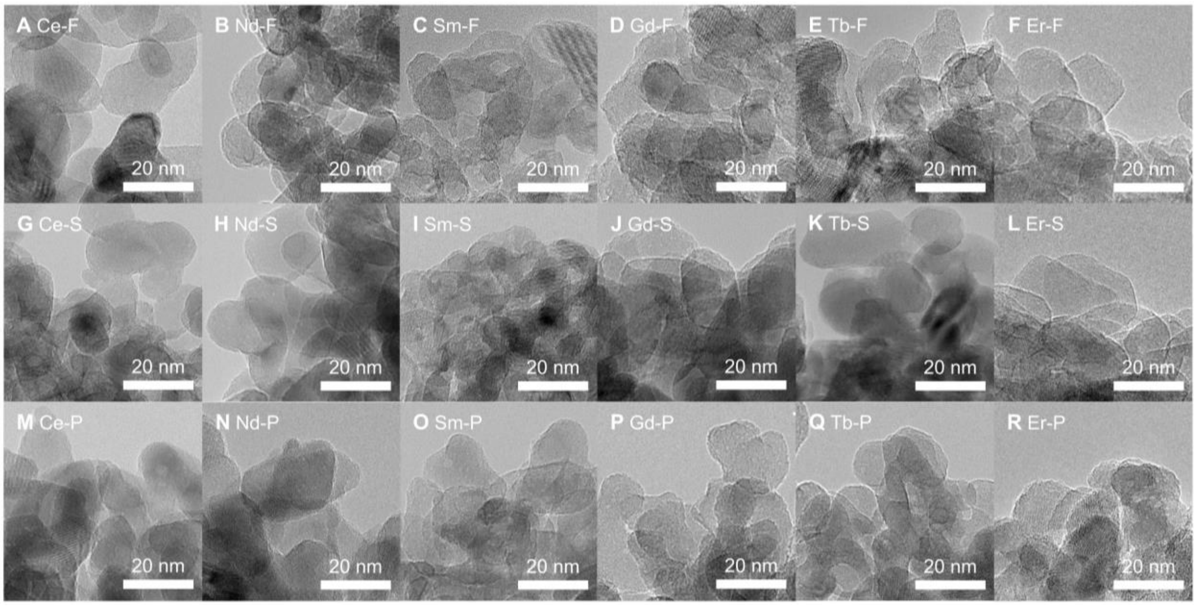

**Fig. S1**. HRTEM images of the catalysts.

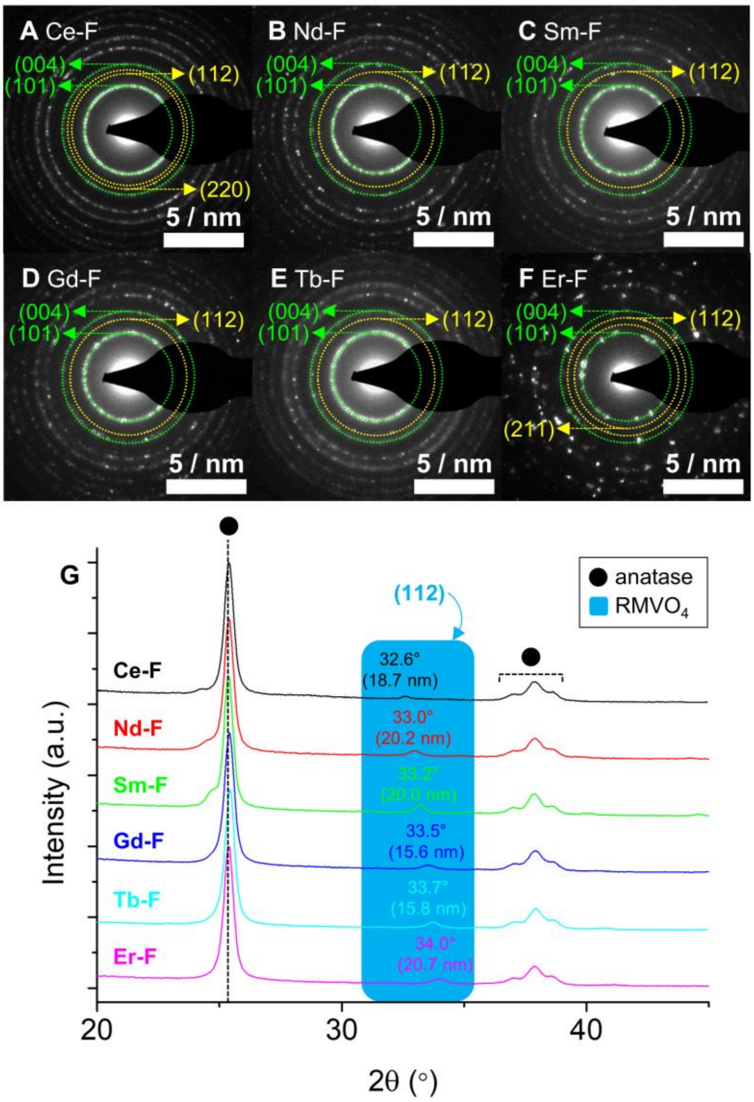

**Fig. S2**. (A-F) SAED patterns of the RM-F catalysts. Green dashed circles indicate the surface facets indexed to those of *tetragonal* anatase ($TiO_2$, JCPDF No. of 01-084-1285), whereas yellow dashed circles indicate the surface facets assigned to those of *tetragonal* $RMVO_4$ (JCPDF No. of 01-072-0282 for $CeVO_4$; 01-072-0280 for $NdVO_4$; 01-072-0279 for $SmVO_4$; 01-072-0277 for $GdVO_4$; 01-072-0276 for $TbVO_4$; 01-072-0337 for $ErVO_4$). (G) XRD patterns of the RM-F catalysts. Black solid circles denote the bulk facets indigenous to *tetragonal* anatase. Domain highlighted with sky-blue indicates the bulk (112) reflections of *tetragonal* $RMVO_4$ phases, whose 2θ values and crystallite sizes are also specified.

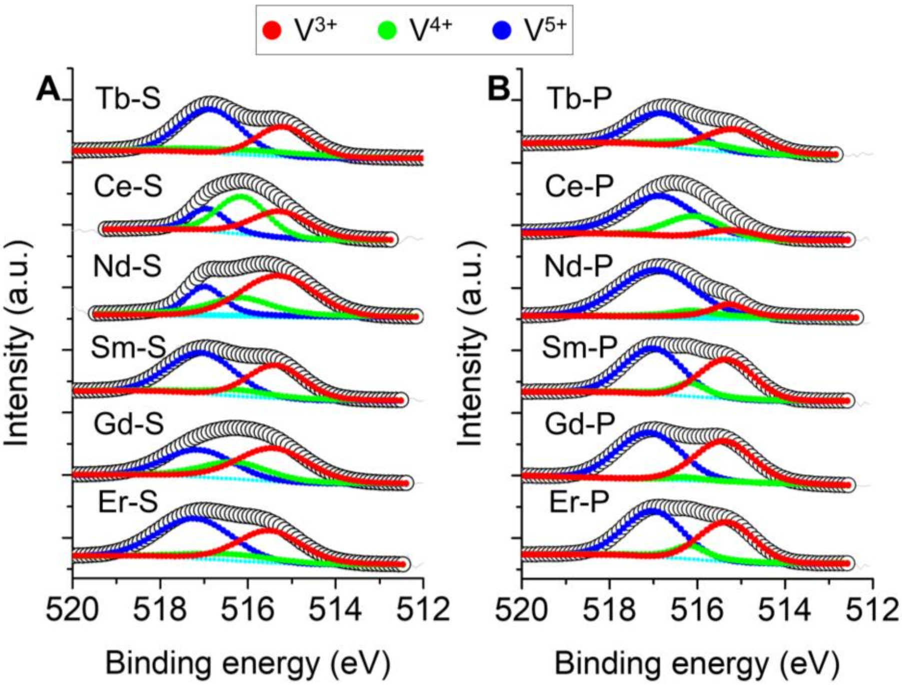

**Fig. S3**. XP spectra of (A) the RM-S and (B) RM-P catalysts in the V 2p $_{3/2}$ regions. Grey solid lines denote raw spectra, whereas black empty and cyan solid circles indicate fitted spectra and backgrounds, respectively. Red, green, and blue solid circles indicate the sub-bands assigned to surface $V^{3+}$, $V^{4+}$, and $V^{5+}$ species, respectively.

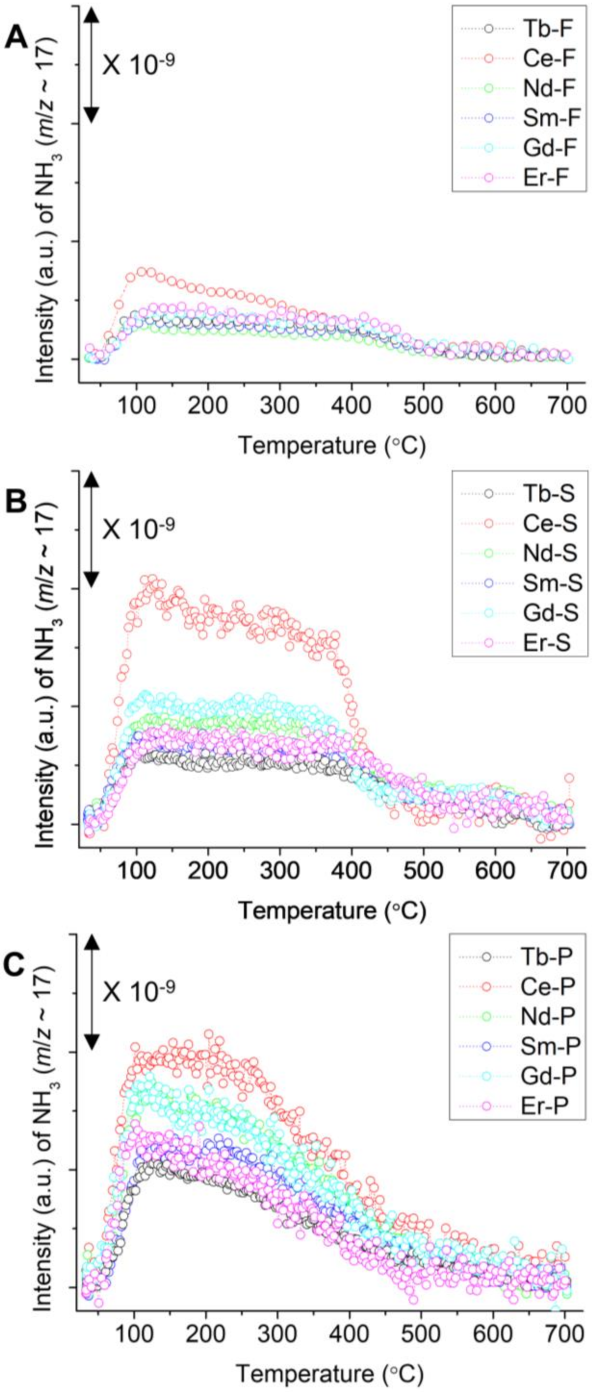

**Fig. S4**. $NH_3$-TPD profiles ($NH_3$ signal versus temperature) of the catalysts after the saturation of their surfaces with $NH_3$ at 35 °C (RM-F for (A); RM-S for (B); RM-P for (C)).

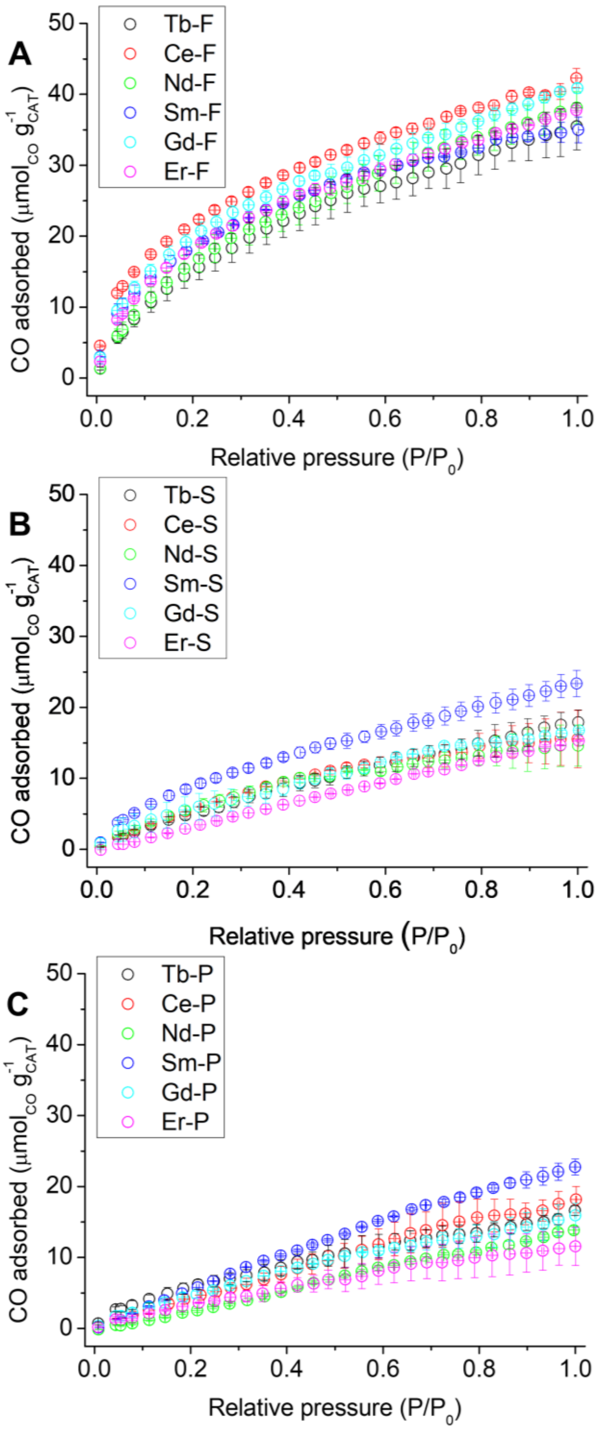

**Fig. S5**. CO isotherms of the catalysts measured at -20 °C (RM-F for (A); RM-S for (B); RM-P for (C)).

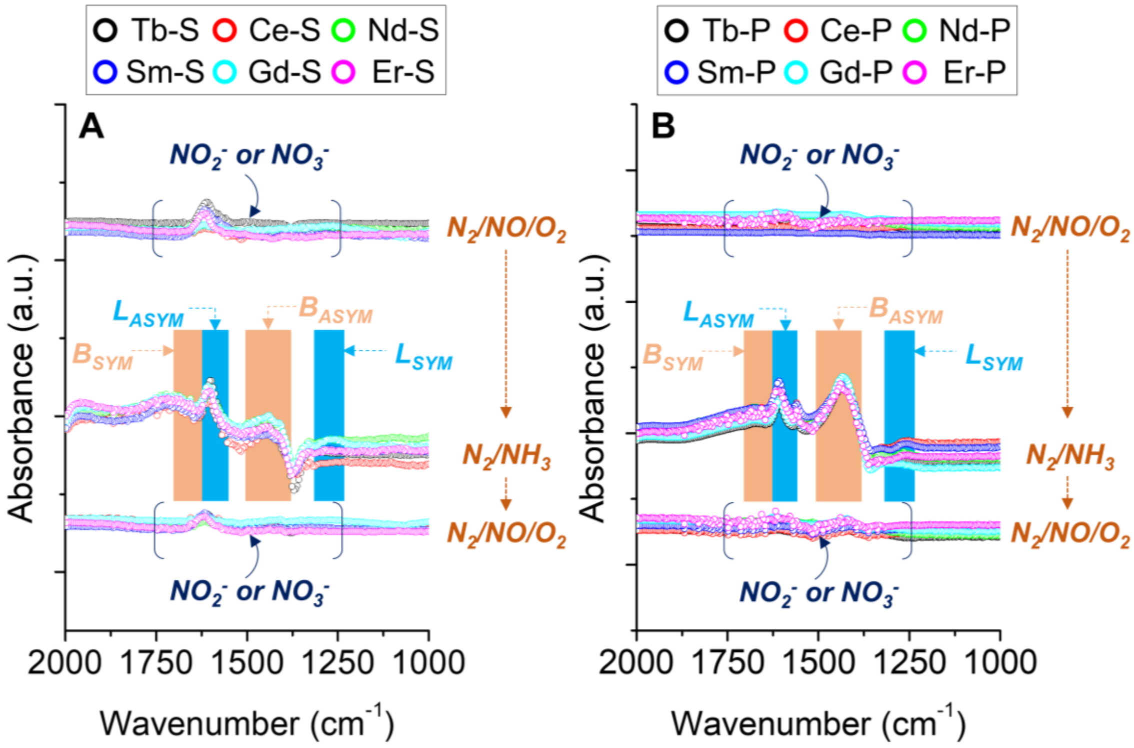

**Fig. S6**. Background-subtracted *in situ* DRIFT spectra of (A) the RM-S and (B) RM-P catalysts after the exposure of their surfaces to the following feed gas streams at 280 °C: 1,000 ppm NO/3 vol. % $O_2$ for 30 minutes (denoted as $N_2/NO/O_2$) → 1,000 ppm $NH_3$ for 30 minutes (denoted as $N_2/NH_3$) → $N_2/NO/O_2$, throughout which $N_2$ served as a balance gas, whereas the total flow rate was 200 mL min$^{-1}$. ***$NO_2^-$/$NO_3^-$*** denotes vibrational signals of N-O bonds belonging to $NO_2^-$/$NO_3^-$ species bound to the surfaces. ***B*** and ***L*** denote symmetric (*SYM*) or asymmetric (*ASYM*) bending vibrational signals of N-H bonds belonging to $NH_3$ species coordinated to surface Brönsted acidic and Lewis acidic sites, respectively.

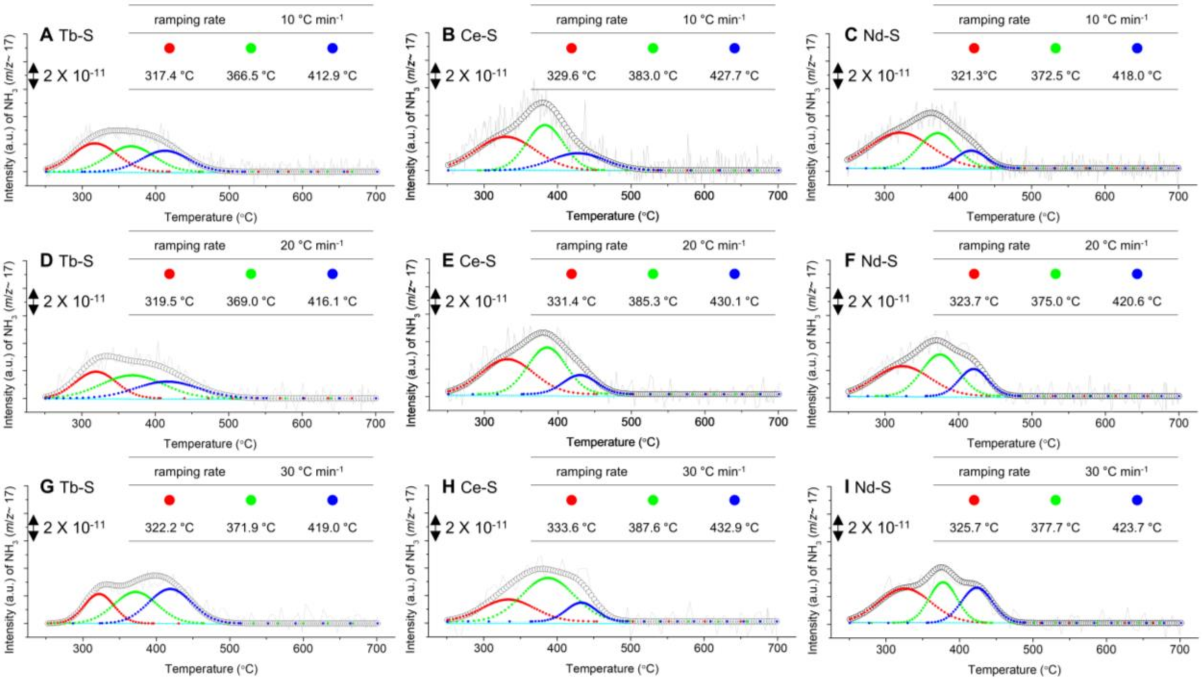

**Fig. S7**. $NH_3$-TPD profiles ($NH_3$ signal versus temperature) of Tb-S (A, D, and G), Ce-S (B, E, and H), and Nd-S (C, F, and I) after the saturation of their surfaces with $NH_3$ at 250 °C with the use of various ramping rates (β) of 10 °C min$^{-1}$ (A-C), 20 °C min$^{-1}$ (D-F), and 30 °C min$^{-1}$ (G-I). Inset tables display the temperatures of the peaks for the sub-bands (denoted as $T_M$) obtained from the deconvolution of the $NH_3$-TPD profiles. (See solid circles marked with red, green, and blue for details.)

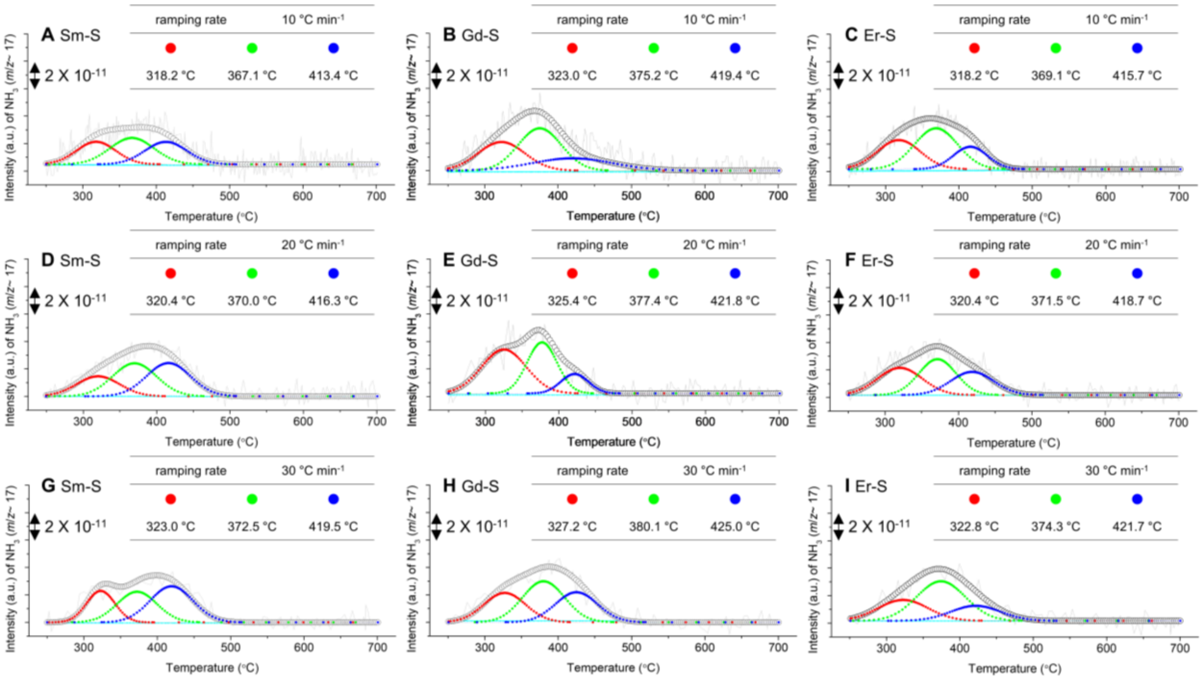

**Fig. S8**. $NH_3$-TPD profiles ($NH_3$ signal versus temperature) of Sm-S (A, D, and G), Gd-S (B, E, and H), and Er-S (C, F, and I) after the saturation of their surfaces with $NH_3$ at 250 °C with the use of various ramping rates (β) of 10 °C min$^{-1}$ (A-C), 20 °C min$^{-1}$ (D-F), and 30 °C min$^{-1}$ (G-I). Inset tables display the temperatures of the peaks for the sub-bands (denoted as $T_M$) obtained from the deconvolution of the $NH_3$-TPD profiles. (See solid circles marked with red, green, and blue for details.)

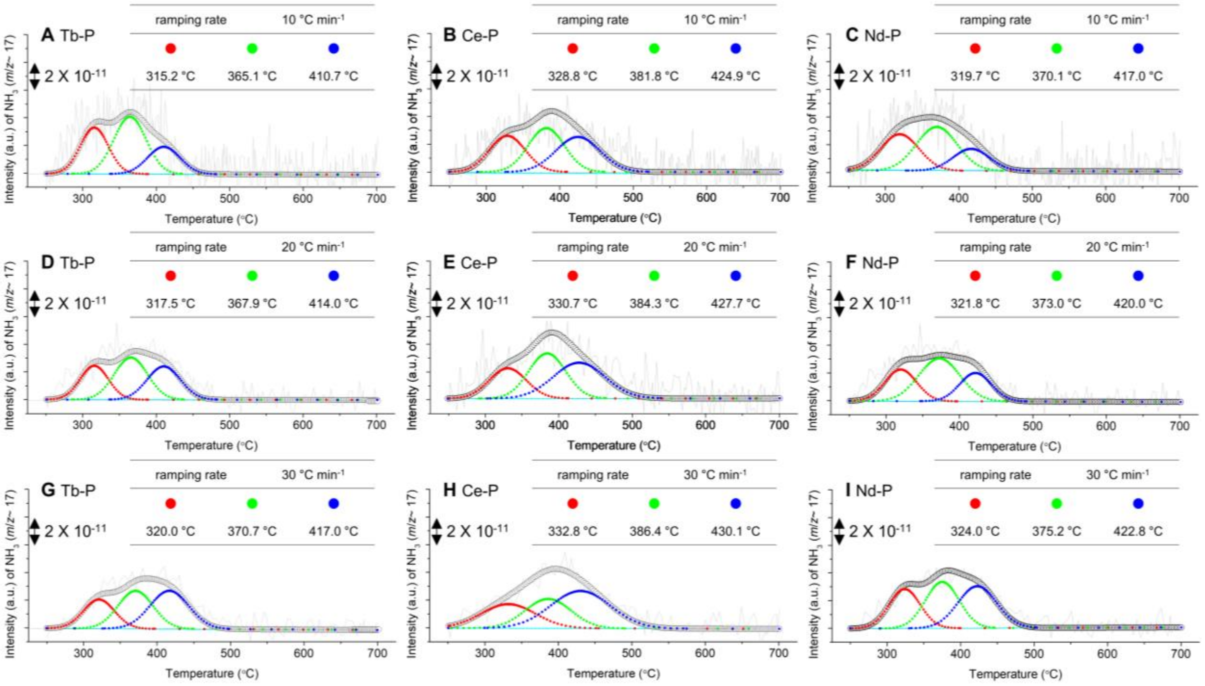

**Fig. S9**. NH$_3$-TPD profiles (NH$_3$ signal versus temperature) of Tb-P (A, D, and G), Ce-P (B, E, and H), and Nd-P (C, F, and I) after the saturation of their surfaces with NH$_3$ at 250 °C with the use of various ramping rates (β) of 10 °C min$^{-1}$ (A-C), 20 °C min$^{-1}$ (D-F), and 30 °C min$^{-1}$ (G-I). Inset tables display the temperatures of the peaks for the sub-bands (denoted as T$_M$) obtained from the deconvolution of the NH$_3$-TPD profiles. (See solid circles marked with red, green, and blue for details.)

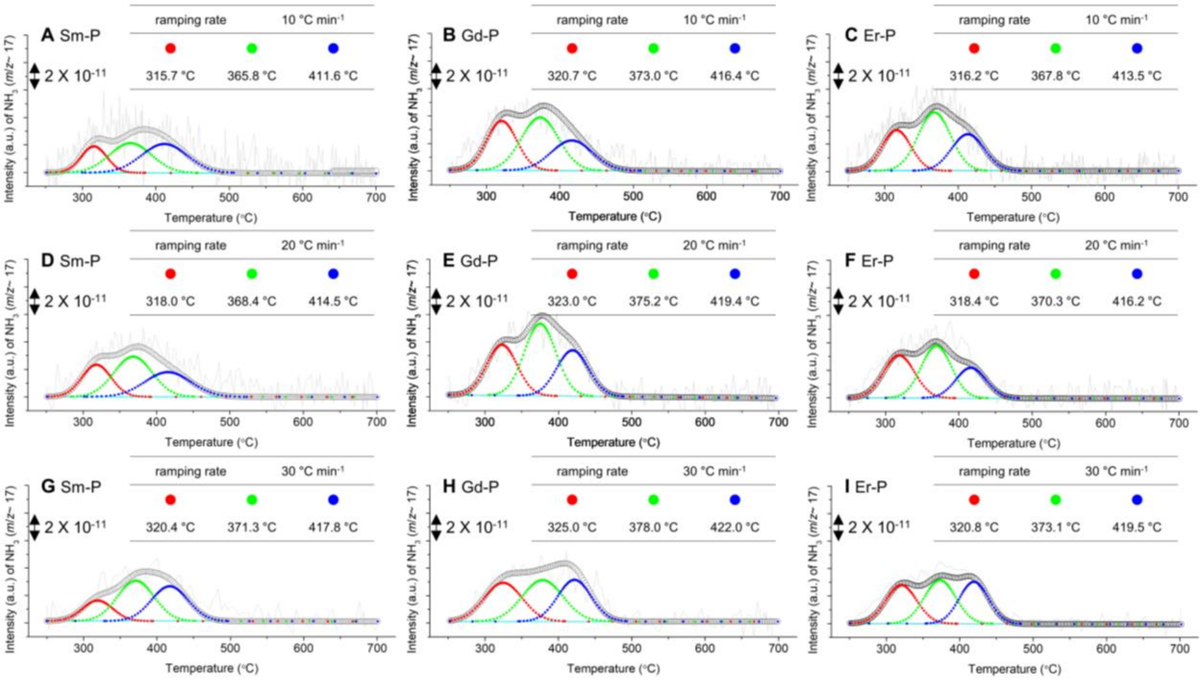

**Fig. S10**. $NH_3$-TPD profiles ($NH_3$ signal versus temperature) of Sm-P (A, D, and G), Gd-P (B, E, and H), and Er-P (C, F, and I) after the saturation of their surfaces with $NH_3$ at 250 °C with the use of various ramping rates (β) of 10 °C min$^{-1}$ (A-C), 20 °C min$^{-1}$ (D-F), and 30 °C min$^{-1}$ (G-I). Inset tables display the temperatures of the peaks for the sub-bands (denoted as $T_M$) obtained from the deconvolution of the $NH_3$-TPD profiles. (See solid circles marked with red, green, and blue for details.)

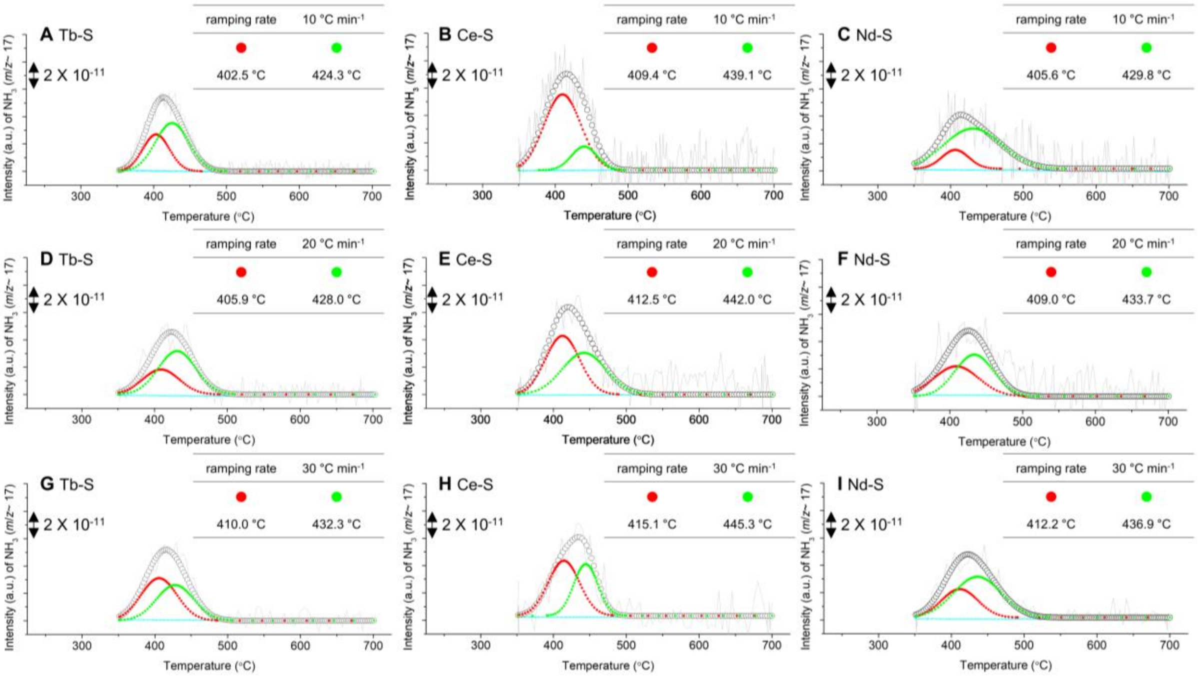

**Fig. S11**. $NH_3$-TPD profiles ($NH_3$ signal versus temperature) of Tb-S (A, D, and G), Ce-S (B, E, and H), and Nd-S (C, F, and I) after the saturation of their surfaces with $NH_3$ at 350 °C with the use of various ramping rates (β) of 10 °C min$^{-1}$ (A-C), 20 °C min$^{-1}$ (D-F), and 30 °C min$^{-1}$ (G-I). Inset tables display the temperatures of the peaks for the sub-bands (denoted as $T_M$) obtained from the deconvolution of the $NH_3$-TPD profiles. (See solid circles marked with red and green for details.)

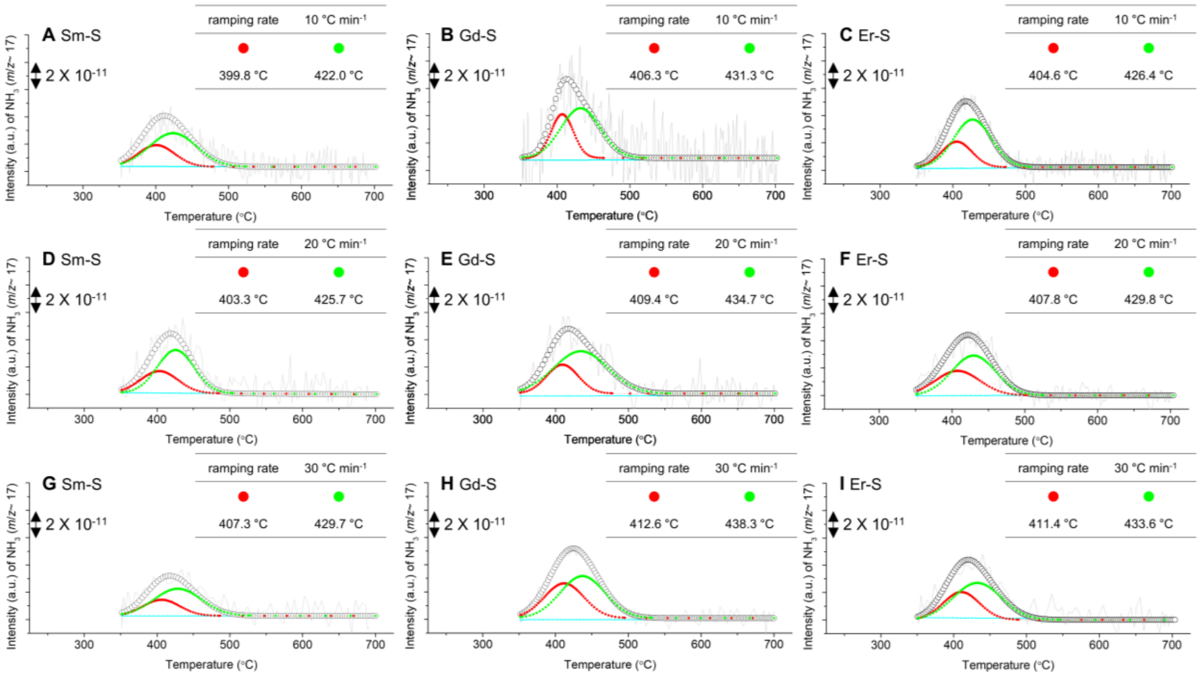

**Fig. S12**. NH$_3$-TPD profiles (NH$_3$ signal versus temperature) of Sm-S (A, D, and G), Gd-S (B, E, and H), and Er-S (C, F, and I) after the saturation of their surfaces with NH$_3$ at 350 °C with the use of various ramping rates (β) of 10 °C min$^{-1}$ (A-C), 20 °C min$^{-1}$ (D-F), and 30 °C min$^{-1}$ (G-I). Inset tables display the temperatures of the peaks for the sub-bands (denoted as T$_M$) obtained from the deconvolution of the NH$_3$-TPD profiles. (See solid circles marked with red and green for details.)

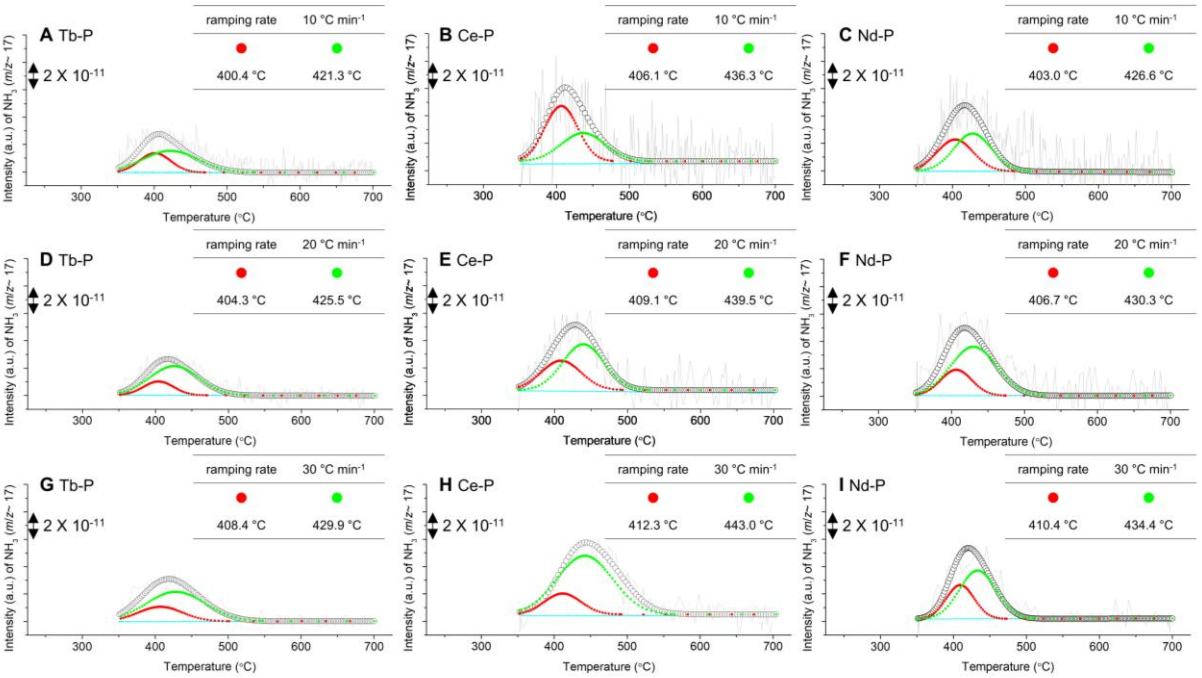

**Fig. S13**. $NH_3$-TPD profiles ($NH_3$ signal versus temperature) of Tb-P (A, D, and G), Ce-P (B, E, and H), and Nd-P (C, F, and I) after the saturation of their surfaces with $NH_3$ at 350 °C with the use of various ramping rates (β) of 10 °C min$^{-1}$ (A-C), 20 °C min$^{-1}$ (D-F), and 30 °C min$^{-1}$ (G-I). Inset tables display the temperatures of the peaks for the sub-bands (denoted as $T_M$) obtained from the deconvolution of the $NH_3$-TPD profiles. (See solid circles marked with red and green for details.)

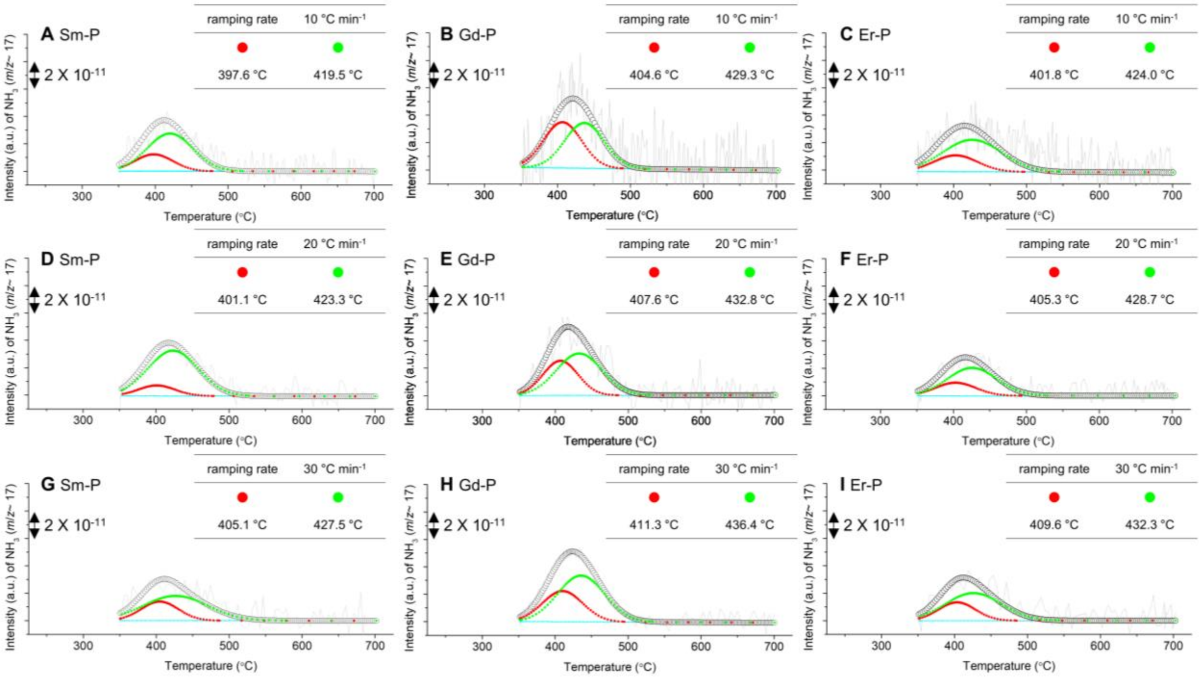

**Fig. S14**. $NH_3$-TPD profiles ($NH_3$ signal versus temperature) of Sm-P (A, D, and G), Gd-P (B, E, and H), and Er-P (C, F, and I) after the saturation of their surfaces with $NH_3$ at 350 °C with the use of various ramping rates (β) of 10 °C min$^{-1}$ (A-C), 20 °C min$^{-1}$ (D-F), and 30 °C min$^{-1}$ (G-I). Inset tables display the temperatures of the peaks for the sub-bands (denoted as $T_M$) obtained from the deconvolution of the $NH_3$-TPD profiles. (See solid circles marked with red and green for details.)

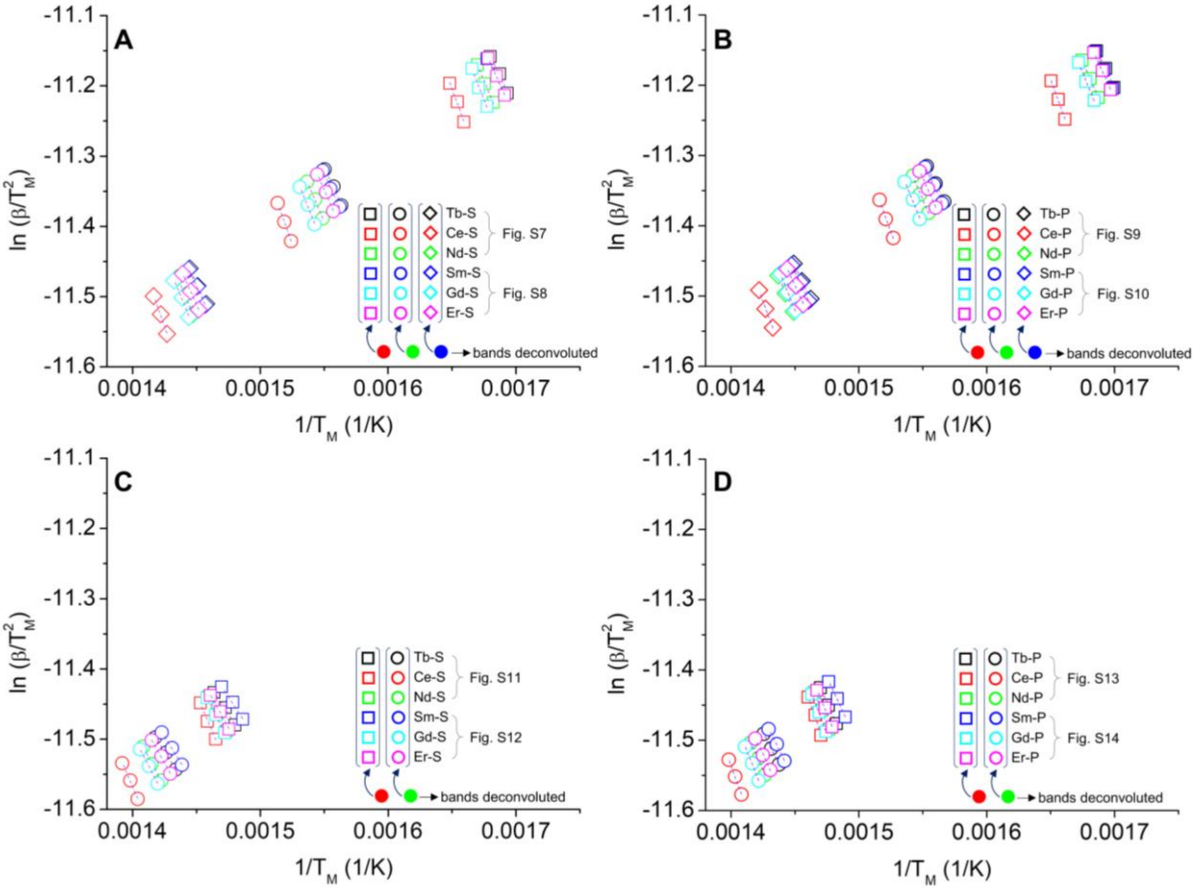

**Fig. S15**. Profiles of ln ($\beta/T_M^2$) versus ($1/T_M$) for the RM-S (A and C) and RM-P catalysts (B and D). β denotes the ramping rate (10-30 °C min$^{-1}$) utilized for the $NH_3$-TPD experiments at ≥ 250 °C (A and B) or ≥ 350 °C (C and D), whereas $T_M$ indicates the peak temperature of the sub-bands obtained through the deconvolution of the $NH_3$-TPD profiles. Violet dashed lines are the fittings (regression factors ($R^2$) of ≥ 0.99) with the slopes of -($E_{NH3}/R$) values, where $E_{NH3}$ and R indicate $NH_3$ binding energy and ideal gas constant, respectively.

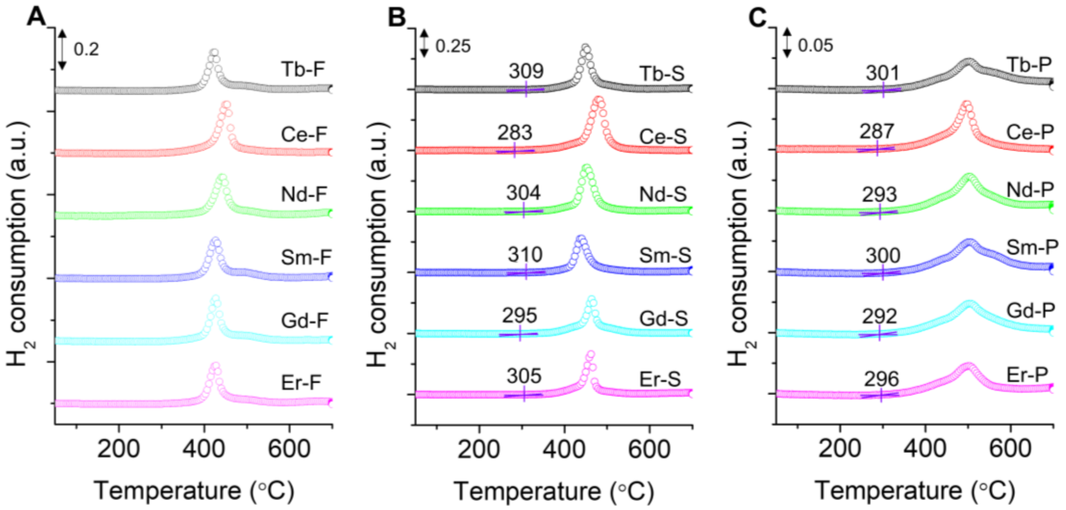

**Fig. S16**. $H_2$-TPR profiles ($H_2$ consumption signal versus temperature) of the catalysts at ≥ 50 °C (RM-F for (A); RM-S for (B); RM-P for (C)). The temperatures shown in (B) and (C) indicate the onsets, at which the catalysts initiated $H_2$ consumption.

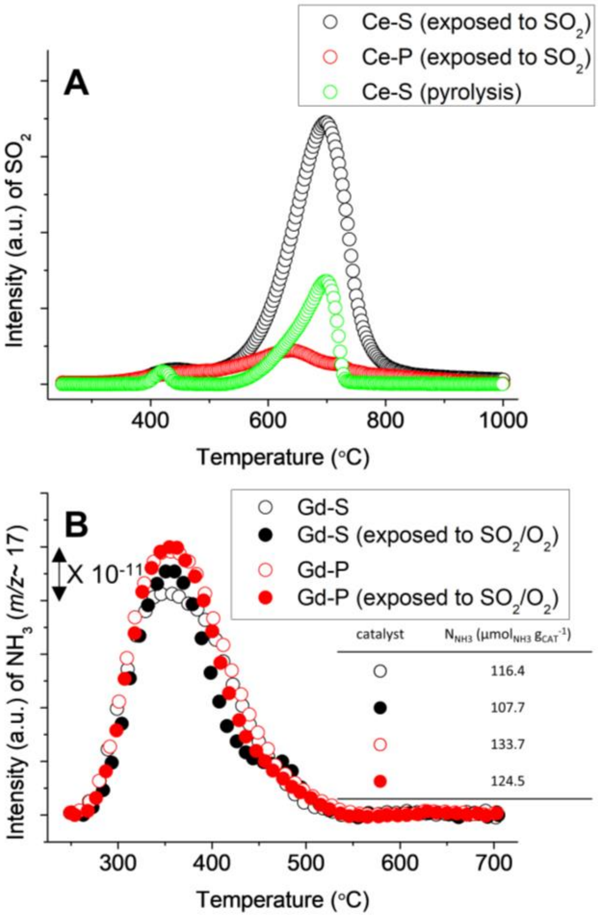

**Fig. S17**. (A) $SO_2$-TPD profiles ($SO_2$ signal versus temperature) of the Ce-S and Ce-P after the saturation of their surfaces with $SO_2$ at 250 °C (denoted as Ce-S (exposed to $SO_2$) and Ce-P (exposed to $SO_2$)). $N_2$-TPD profile of the Ce-S unsubjected to the saturation of its surface with $SO_2$ at 250 °C (denoted as Ce-S (pyrolysis)). (B) $NH_3$-TPD profiles ($NH_3$ signal versus temperature) of the Gd-S, Gd-P, and their analogues exposed to 500 ppm $SO_2$/3 vol. % $O_2/N_2$ with the space velocity of 30,000 $hr^{-1}$ and the total flow rate of 500 mL $min^{-1}$ at 250 °C for 10 hours. Inset table exhibits the amounts of $NH_3$ adsorbed per gram of catalysts with $NH_3$ adsorption temperature of 250 °C.

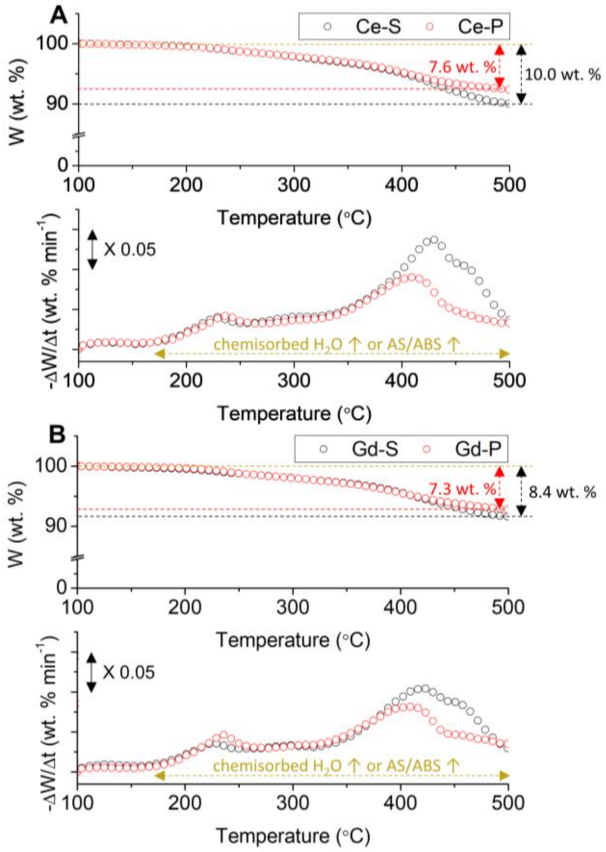

**Fig. S18**. TGA and DTG profiles of (A) the Ce-S/Ce-P and (B) Gd-S/Gd-P, all of which were exposed to a $N_2$-balanced flue gas stream consisting of $NO_X$ (800 ppm), $NH_3$ (800 ppm), $O_2$ (3 vol. %), $H_2O$ (6 vol. %), and $SO_2$ (500 ppm) with the space velocity of 60,000 $hr^{-1}$ and the total flow rate of 500 mL $min^{-1}$ at 180 °C for 24 hours.